Eur. Phys. J. B **61**, 445–455 (2008)
DOI: 10.1140/epjb/e2008-00105-2

THE EUROPEAN PHYSICAL JOURNAL B

Weak temperature gradient effect on the stability of the circular Couette flow

V. Lepiller[1], A. Goharzadeh[2], A. Prigent[1], and I. Mutabazi[1,a]

[1] Laboratoire d'Ondes et Milieux Complexes (LOMC), FRE 3102, CNRS-Université du Havre, 25 rue Philippe Lebon, 76058 Le Havre Cedex, France
[2] Mechanical Engineering Department, The Petroleum Institute, PO Box 2533 Abu Dhabi, UAE

Received 14 September 2007 / Received in final form 28 December 2007
Published online 13 March 2008 –

Abstract. We have investigated the influence of a weak radial temperature gradient in a wide gap and large aspect ratio Couette-Taylor system. The inner cylinder is rotating and can be heated or cooled, the outer cylinder is at rest and immersed in a large thermal bath. We found that a radial temperature gradient destabilizes the Couette flow leading to a pattern of traveling helicoidal vortices occurring only near the bottom of the system. The size of the pattern increases as the rotation frequency of the cylinder is increased. We have characterized the spatiotemporal properties of the pattern and we have shown that it behaves as a wall mode found in the simulation of the complex Ginzburg-Landau equation with homogeneous boundary conditions.

PACS. 47.20.Qr Centrifugal instabilities (e.g., Taylor-Couette flow) – 47.50.Qj Instabilities – 47.54.-r Pattern selection; pattern formation – 82.40. Pattern formation in flow and heat transfer

1 Introduction

The stability of the circular Couette flow in a vertical cylindrical annulus submitted to a radial temperature gradient has been the subject of large number of theoretical, experimental and numerical studies in last decades [1–3]. This problem occurs in many industrial applications such as electrical motors [4,5] or barrel reactors used in the chemical vapor deposition [6]. Moreover, this flow system occurs in geophysical applications with oceanic or atmospheric circulation [7]. Among the few experimental studies, Snyder and Karlsson [8] have performed investigations in a tall vertical annulus with a small gap to understand the influence of radial temperature heating on the stability of the flow for three different Prandtl numbers. They have observed that small positive and negative radial temperature gradient stabilizes the base flow. For larger temperature gradient, the flow is destabilized and spiral vortices were observed. In their experiment, Sorour and Coney [9] have found that the imposed radial temperature gradient destabilizes the base flow and the obtained pattern is composed of stationary axisymmetric toroidal vortices. Although they did not provide the values of the Prandtl number for the used oils, their values were given by Ali and Weidman [10], $Pr \in \{300; 860\}$. Ball et al. [7] have shown different successive regimes for system with a moderate aspect ratio for air. The previous studies have underlined the importance and the complexity of the problem depending both on the nature of the fluid and the size of the cavity. As the previous studies were limited to visualization, the present work provides pictures of the pattern and more quantitative data (wavenumber, frequency, amplitude) using the analysis of space-time diagrams. The chosen aspect ratio is very large to avoid boundary effects. We have worked with the same range of temperature gradient values as Snyder and Karlsson or Sorour and Coney, but the range of Grashof number values is larger because of a larger gap size. We have characterized in detail the primary bifurcation for small values of the Grashof number. We have found significantly different results from previous studies; in particular, we have observed the wall mode that was predicted by Tobias et al. [11] in numerical simulations of 1-d CGLE (complex Ginzburg-Landau equation) with homogeneous boundary conditions. Snyder et al. [12] have provided a large work on the Taylor Couette system in different conditions, particularly with a through axial flow. They invoked a parallel between these two behaviors. We have pursued these observations to compare our results with the recent experiments of Tsameret et al. [13–16] and Babcock et al. [17,18]. Although these works were focused on the absolute and convective instabilities, several similar behaviors are observable. The paper is organized as follows. The problem formulation is presented in Section 2. The experimental setup and the results are presented respectively in Sections 3 and 4. In Section 5, the results are discussed and finally the last section contains the conclusion.

[a] e-mail: mutabazi@univ-lehavre.fr

2 Theoretical background

A Newtonian fluid is confined between an inner cylinder of radius a that has an angular velocity Ω_i and an outer fixed cylinder of radius b. The two cylinders of length L are maintained at the temperature T_1 and T_2 respectively. Equations governing the motion of the fluid are the Navier-Stokes equations, the continuity equation and the energy conservation for the velocity $\mathbf{v}$, the pressure p and the temperature T [19]. The Boussinesq approximation is used. The temperature difference between the two cylinders produces a radial stratification of density inducing a torque that generates a large vertical convection cell. The flow is ascending near the hot surface and descending near the cool one. The rotation of the inner cylinder induces a circular Couette flow with a radial stratification of the kinetic momentum. Far from the top and bottom boundaries, the base flow is stationary and has two velocity components: an azimuthal velocity component due to the rotation [1]

$$V_\theta(\bar{r}) = A\bar{r} + B/\bar{r} \tag{1}$$

with

$$\bar{r} = \frac{r}{d} \quad , \quad A = -\frac{\Omega_i a \eta}{1+\eta} \quad , \quad B = \frac{\Omega_i a}{(1-\eta)^2} \quad , \quad \eta = \frac{a}{b}$$

and an axial component induced by the radial temperature gradient [10]

$$W(\bar{r}) = W_a F(\eta, \bar{r}) \quad , \quad W_a = \frac{g\alpha\delta T d^2}{\nu} \tag{2}$$

with

$$F(\eta,\bar{r}) = C\Bigg\{ D\left[(1-\eta^2)\bar{r}^2 - 1 + (1-\eta^2)\frac{\ln[(1-\eta)\bar{r}]}{\ln\eta}\right] - 4\left[\bar{r}^2(1-\eta)^2 - \eta^2\right]\frac{\ln[(1-\eta)\bar{r}]}{\ln\eta}\Bigg\}$$

where

$$C = \frac{1}{16(1-\eta^2)}$$
$$D = \frac{(1-\eta^2)(1-3\eta^2) - 4\eta^4 \ln\eta}{(1-\eta^2)^2 + (1-\eta^4)\ln\eta}.$$

The function $F(\eta,\bar{r})$ does not depend on the radial temperature gradient. It possesses a nodal surface $r = r_0(\eta)$ and it reaches the maximum for $x_{max}(\eta)$ and the minimum for $x_{min}(\eta)$ where we have set $x = (r-a)/d$ (Fig. 1). Some of these values are given in Table 1 for few experimental systems for comparison.

The temperature field T depends only on the radial coordinate $\bar{r}$ as follows (Fig. 2):

$$\Theta(\bar{r}) = \frac{T(\bar{r}) - T_2}{(T_1 - T_2)} = \frac{\ln[(1-\eta)\bar{r}]}{\ln\eta} \tag{3}$$

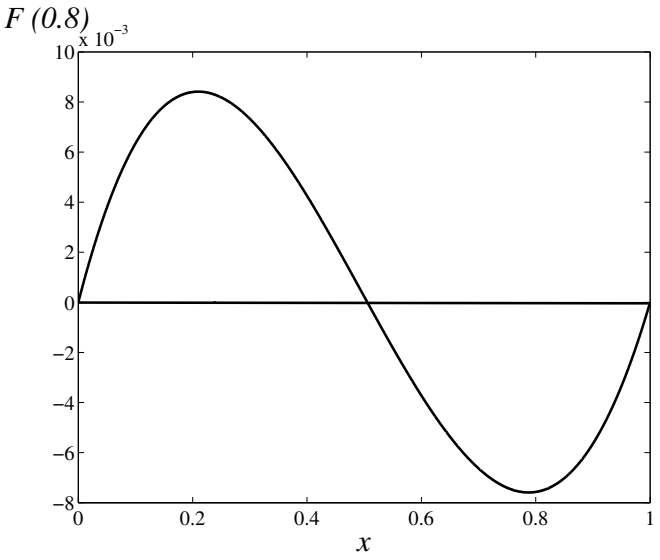

Fig. 1. Radial profile of the dimensionless axial velocity $F(\eta,\bar{r})$ for $\eta = 0.8$.

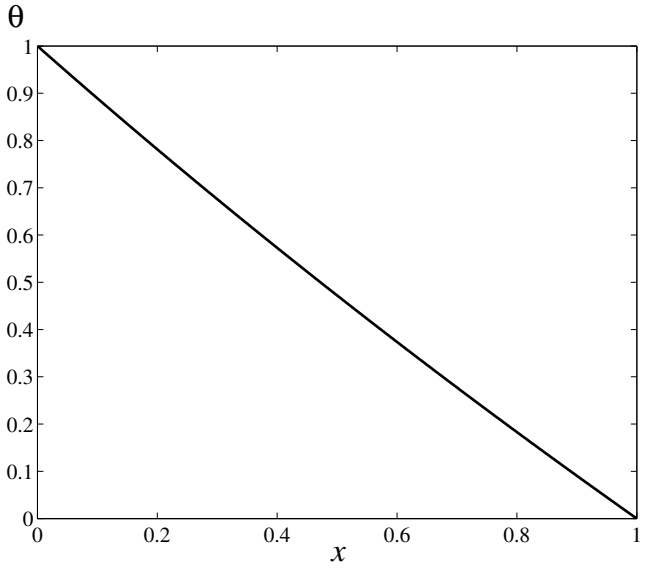

Fig. 2. Radial profile of the temperature $\theta(x)$ for $\eta = 0.8$.

The flow in this system is controlled by five parameters. Two geometrical parameters, i.e. the radius ratio η and the aspect ratio $\Gamma = L/(b-a)$, and three physical parameters, i.e. the Taylor number Ta, the Grashof number Gr and the Prandtl number Pr. The Taylor number is given by the ratio of the viscous diffusion time $\tau_\nu = d^2/\nu$ to the characteristic time of the centrifugal force $\tau_c = \Omega^{-1}(d/a)^{1/2}$, $Ta = \tau_\nu/\tau_c = (\Omega a d/\nu)\sqrt{d/a}$. The Grashof number, related to buoyancy effects, is the squared ratio of the viscous diffusion time to the characteristic time related to buoyancy $\tau_a = \sqrt{d/g\alpha\delta T}$, $Gr = \tau_\nu^2/\tau_a^2 = g\alpha\delta T d^3/\nu^2$.

Table 1. Typical values of the function $F(\eta, \bar{r})$ for different experimental studies.

Authors	η	d (cm)	x_{min}	x_{max}	$10^3 F_{min}$	$10^3 F_{max}$
Snyder et al. [8]	0.958	0.267	0.793	0.210	−7.9	8.1
Sorour et al. [9]	0.911	1.02	0.786	0.209	−7.8	8.2
	0.948	0.6	0.788	0.211	−7.9	8.2
Ball et al. [7]	0.437	1.611	0.787	0.204	−6.4	9.2
	0.565	0.964	0.787	0.207	−6.9	8.9
	0.656	0.656	0.787	0.208	−7.2	8.7
This study	0.8	0.5	0.788	0.215	−7.6	8.4

The Prandtl number is the ratio of thermal diffusion time to viscous diffusion time: $Pr = \tau_\kappa/\tau_\nu = \nu/\kappa$.

3 Experimental setup

3.1 Description

The experimental setup (Fig. 3) is composed of two concentric vertical cylinders of length $L = 57$ cm and thickness $e = 0.5$ cm. The working liquid, demineralized water, is confined between the inner cylinder of radius $a = 2$ cm and the outer cylinder of radius $b = 2.5$ cm. The gap size is $d = 0.5$ cm. The system is characterized by the radii ratio $\eta = 0.8$ and the aspect ratio $\Gamma = 114$. The inner cylinder was driven by a step motor and rotated with angular frequency Ω_i, the outer cylinder was held fixed. Stationary horizontal end plates were used to seal the annulus. The system was surrounded by a large cylindrical glass tank of radius $c = 5$ cm which ensured the thermal insulation from external environment. The temperatures of inner and outer cylinders were controlled by two independent thermal baths. A constant temperature water circulated at flow rate of 250 cm^3/s inside the inner cylinder and between the peripheral cylinders at temperature values T_1 and T_2 respectively. We have checked the absence of the vertical temperature gradient using two thermal sensors inserted at the entry (bottom) and the exit (top) of the experiment. The temperature gradient δT acting on the annulus was obtained by considering the conductivity of aluminium of inner cylinder, of water in the gap and of glass of the outer cylinder and it was given by $\delta T = 0.54\ (T_1 - T_2)$ [20]. The accuracy of the angular velocity of the inner cylinder was 1%.

3.2 Visualization

The visualization was achieved by seeding the flow with a solution containing 2% by volume of Kalliroscope AQ 1000 concentrate [1] [21], a suspension of 1–2% of microscopic reflective and anisotropic platelets that orient themselves parallel to the shear. A monochromatic He-Ne laser beam was transformed by a cylindrical lens into a plane vertical beam parallel to the cylinder axis and allowed for the visualization of a vertical cross section of the flow. A linear CCD camera recorded at regular time intervals the intensity distribution of the light reflected by Kalliroscope flakes along the cross section of 55 cm of the height. The intensity was sampled into 256 grey levels. The recorded lines were superimposed along the time axis to form a space time diagram. Two plane mirrors surrounded the experimental apparatus in order to visualize the whole flow and to determine the inclination angle of vortices [22,23].

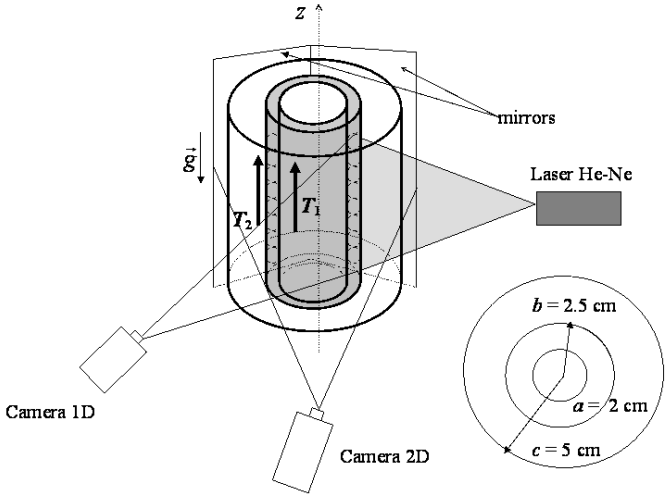

Fig. 3. Schematic representation of the experimental setup.

3.3 Complex demodulation

Analysis of space-time diagrams allows for identification of transition scenarios between the different flow regimes. In order to obtain more quantitative information, the standard demodulation technique was applied to the space–time diagrams $I(z,t)$. A Fourier transform, a space and time wide band-pass filtering of the data around the positive fundamental frequency ω_0 and wavenumber k_0 in Fourier space and then the inverse Fourier transform were performed [24]. The intensity $I(z,t)$ was written in terms

[1] Kalliroscope Corporation, 264 Main Street, PO Box 60, Groton, MA 01450, USA. Kalliroscope.

of a slowly varying complex field $I(z,t) = |A(z,t)|e^{i\phi(z,t)}$ where $|A(z,t)|$ is the modulus of the signal amplitude, and ϕ its phase. Spatial and temporal derivatives of the phase ϕ give the local instantaneous wavenumbers $k = \partial\phi/\partial z$ and frequencies $\omega = -\partial\phi/\partial t$ of the pattern. In the following, we will use the dimensionless wavenumber and frequency defined as follows $q = kd$, $f = d^2\omega/2\pi\nu$. The lengths are expressed in units of d (except the pattern lengths that will be scaled by the working length L).

3.4 Protocol

At the beginning of experiments, a radial temperature gradient was imposed and maintained constant during all the experiment. The outer cylinder was maintained at the temperature $T_2 = 30\,^{\circ}\mathrm{C}$ and we can heat or cool the inner cylinder. As soon as a small radial temperature gradient was imposed on the liquid, the convection cell was created: fluid particles moved upwards near the heated cylindrical wall and moved downwards near the cooled one. After one hour, we gradually increased the angular velocity of the inner cylinder from the rest. This rotation is always in the positive direction (counterclockwise) in this work, although we have observed the same nature of patterns for negative direction. For each increase of the rotational speed, a space-time diagram and a movie of the whole flow were recorded. For each step, we have waited a minimum of twenty minutes before recording a space-time diagram and before increasing the angular velocity. This time step is quite enough to avoid transient effects since the viscous diffusion time across the gap is about 20 s, the characteristic time related to buoyancy is smaller than 2 s and the centrifugal time is about 1 min.

4 Results

The working fluid (deionized water) in the range of values of the experiment temperature has $Pr = 5.5 \pm 0.2$. Based on the stability analysis performed by Walowit et al. [25], the critical Taylor number for an infinite annulus in the isothermal case is $Ta_c^{th} = 47.37$ for $\eta = 0.8$. We have found, for our experimental system ($\Gamma = 114, \eta = 0.8$), the instability threshold is $Ta_c = 48$. Below this value, the base flow is circular Couette flow with a velocity profile given by equation (1) away from the end plates. Above Ta_c, the flow is composed of axisymmetric stationary toroidal vortices i.e. Taylor vortices with the wavenumber $q = 3.12$. With an applied temperature gradient, the critical parameters and the nature of the pattern changed.

4.1 Description of pattern

For $Gr \neq 0$ and at a critical value Ta_c of the Taylor number, the base flow is destabilized and a pattern, composed of non axisymmetric traveling vortices, appears at the bottom of the system. Figures 4a shows a piece of the pattern and the corresponding space-time diagram obtained

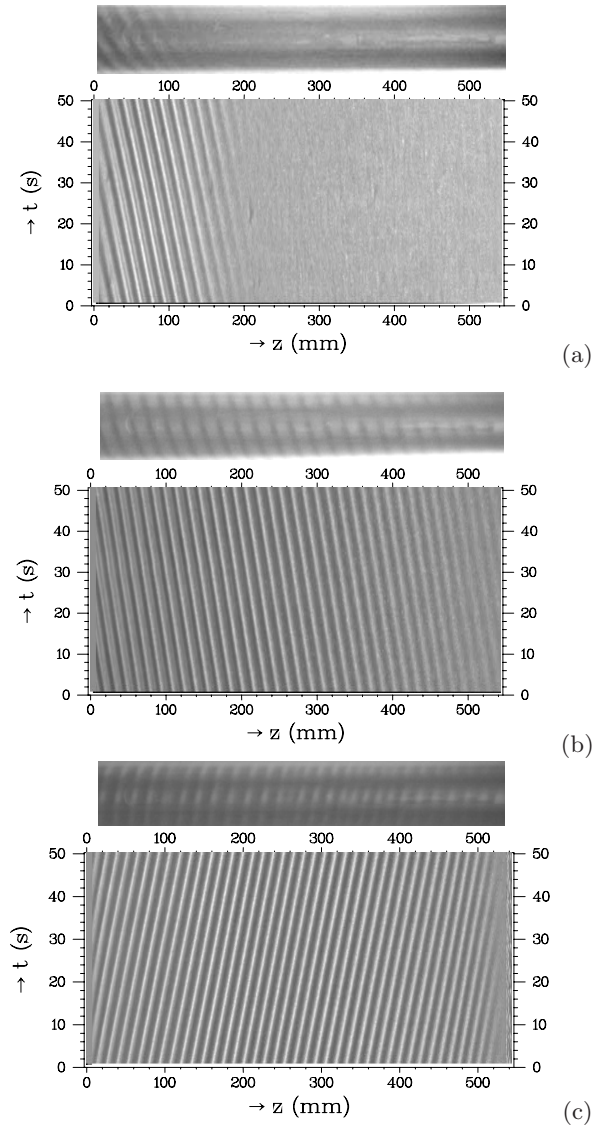

Fig. 4. Pictures and space-time diagram representing the spiral vortex flow for $Gr = 390$ (a) at the threshold for $Ta_c = 27.5$, (b) for $Ta^* = 38.5$ and (c) for $Gr = -420$ and $Ta^* = 37$.

for $Gr = 390$ and $Ta_c = 27.5$. This state is not transient, the pattern size remains constant in time. This Hopf bifurcation is supercritical, no hysteresis effects have been observed when increasing and decreasing the Taylor number near the threshold.

When Ta increases, the size L_p of the pattern [2] increases, the pattern fills the whole system (Fig. 4b) at the value Ta^* of the Taylor number. Thus between Ta_c and Ta^*, there is a coexistence of two states: the laminar base flow and the pattern of traveling vortices. These two states are separated by a front whose positions z_f depends on Ta. Figure 4b shows a pattern with a definite inclination with respect to the plane perpendicular to the cylinder axis, and a propagation from the top to the bottom of the

[2] We have defined the pattern size as the distance between two points where the amplitude is one third of the maximum.

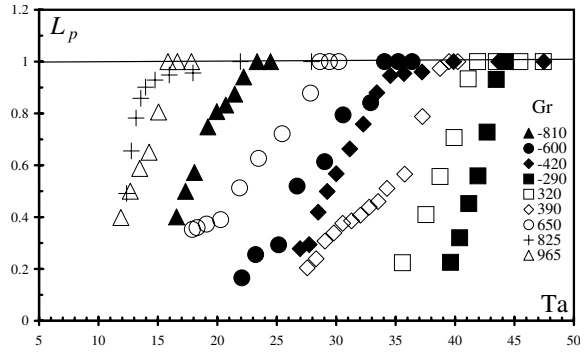

Fig. 5. Variation of the pattern length L_p scaled by the height of the cylinders vs. the Taylor number for different Grashof numbers.

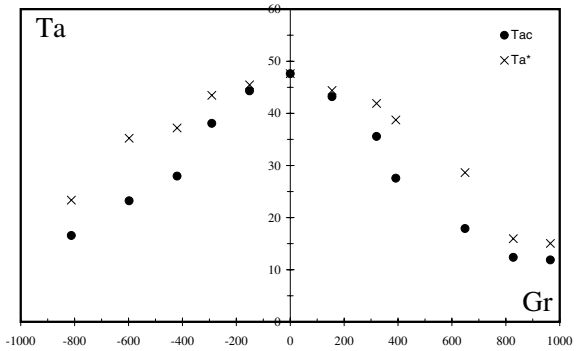

Fig. 6. Variation of the critical Taylor number vs. the Grashof number. The symbols • and × correspond respectively to the value of the Taylor number at the threshold and to that for which the spiral vortex flow fills the whole annulus.

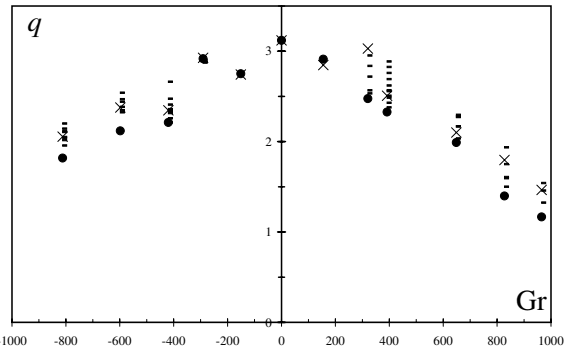

Fig. 7. Variation of the critical wavenumber vs. the Grashof number. At threshold, the wavenumber of the pattern is represented by the symbol •, then by − for increasing Ta. The symbol × corresponds to the wavenumber when the spiral is present in the whole system.

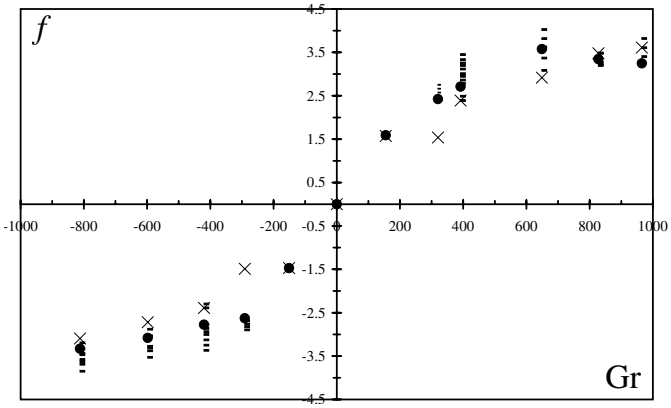

Fig. 8. Variation of the frequency with The Grashof number. At threshold, the frequency of the pattern is represented by the symbol •, then by − for increasing Ta. The symbol × corresponds to the frequency when the spiral is present in the whole system.

cavity. When we changed either the sign of the temperature gradient or the sense of rotation, the inclination of the pattern changed too (Fig. 4c). In order to conserve the pattern inclination, we needed to change simultaneously the sign of both the rotation and temperature gradient.

Figure 5 displays the variation of the pattern size L_p as a function of the Taylor number for each value of Gr.

Figure 6 shows the critical values Ta_c and Ta^* as function of Gr. The critical value of the Taylor number decreases with the Grashof number, i.e. the presence of a radial temperature gradient destabilizes the flow. The spiral pattern remains stable until it pertains a bifurcation to wavy spiral vortex flow, the later exists in a small range of Ta and then becomes wavy vortex flow which is similar to that observed in the isothermal case [2]. For $Gr > 965$, the pattern occurs in the middle of the system with a finite size $L_p \approx L$. The corresponding results will be discussed in another work.

In order to describe the space-time characteristics of the pattern, we have extracted the axial wavenumber and frequency from space-time diagrams. Figures 7 and 8 represent the variation of the wavenumber q and frequency f as functions of the Grashof number Gr. We have found that the axial wavenumber decreases with the Grashof number, i.e. the radial heating increases the axial vortex size, which remains larger than that of the Taylor vortices. The pattern frequency increases with the control parameter, i.e. the radial heating increases the vortex phase velocity.

We have also observed that the azimuthal wavenumber decreases with the Taylor number (Fig. 9). The azimuthal wavenumber is proportional to the inclination of the vortices $m = 2\pi(a+b)\lambda^{-1}\tan\theta$, where θ is the inclination angle of vortices, $\lambda = 2\pi d/q$ is the axial wavelength. For large values of the Grashof number, the pattern is very inclined ($m = 9$ or $\theta = 39.8°$) at the onset and for small Grashof number, the spiral vortex flow is weakly inclined ($m = 1$ or $\theta = 2°$). For the same value of the Taylor number, the azimuthal wavenumber also depends on the Grashof number. Moreover, the ratio between frequency and azimuthal wavenumber, i.e. the azimuthal phase speed c_θ, increases with the Taylor number Ta whatever the value of the Grashof number Gr is as shown Figure 10.

The amplitude profile of the pattern $\langle A(z)\rangle$ obtained from demodulation and averaged in time is plotted in Figure 11 for a fixed value of Gr and different values of the reduced Taylor number $\mu = (Ta - Ta_c(Gr))/Ta_c(Gr)$.

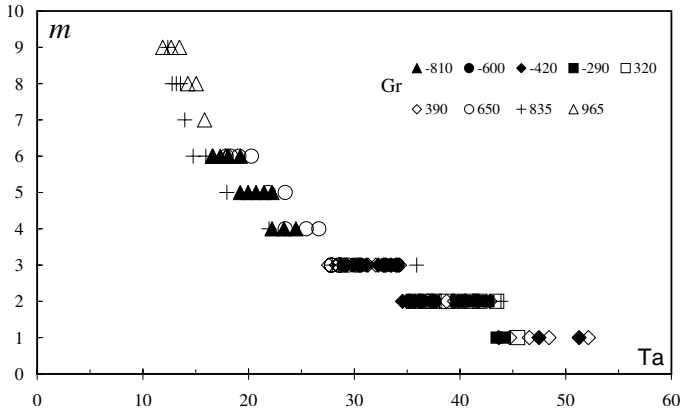

Fig. 9. Variation of the azimuthal wavenumber vs. the Taylor number for different Grashof number.

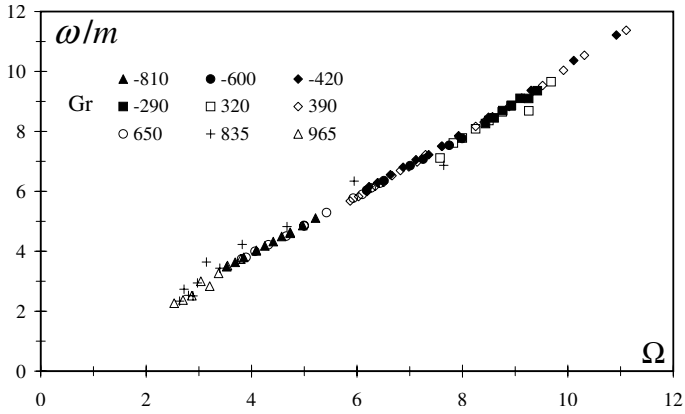

Fig. 10. Variation of the ratio ω/m vs. the mean rotation rate of the inner cylinder Ω.

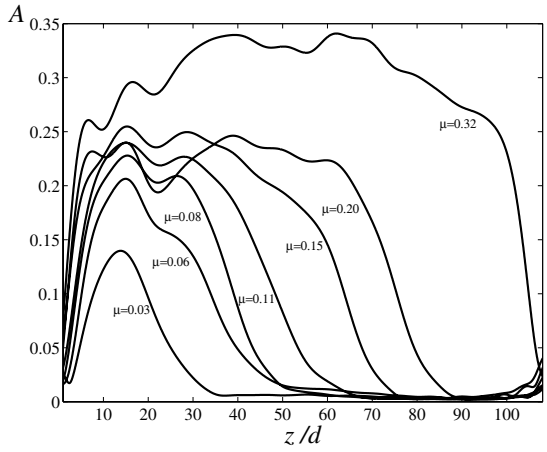

Fig. 11. Time-averaged amplitude profiles of the spirals for $Gr = -420$ and different values of μ.

Time-averaged profiles of the frequency and the axial wavenumber are plotted in Figures 12 and 13.

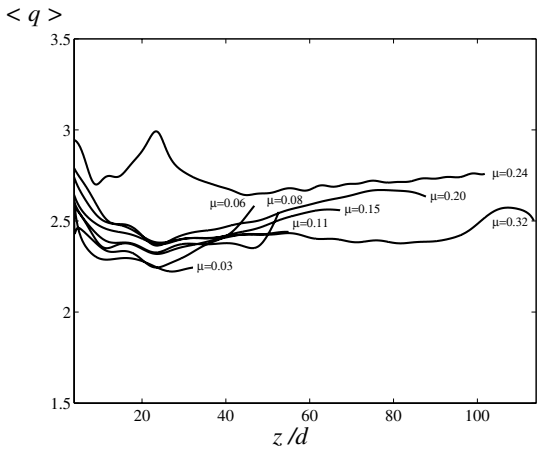

Fig. 12. Time-averaged profiles of the wavenumber for $Gr = -420$ and different values of μ.

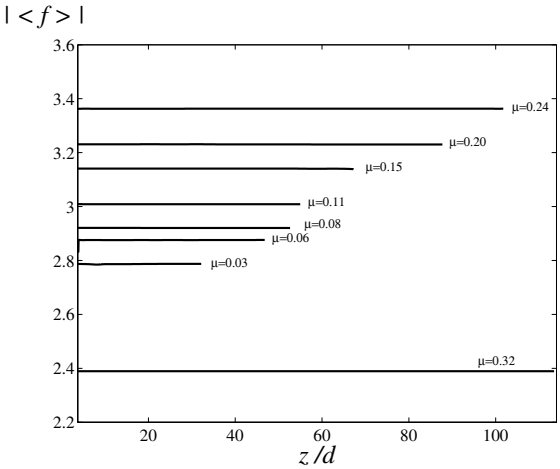

Fig. 13. Time-averaged profiles of the frequency for $Gr = -420$ and different values of μ.

5 Discussion

5.1 Pattern near the bottom

The occurrence of the pattern near the bottom of the system independently of the sign of the temperature gradient and of the rotation may be due to the modification of the Ekman zones near the end plates. In fact, near these ends, the large convection cell induced by the radial temperature gradient introduces an extra radial velocity component and an axial velocity component that does not exist in the isothermal case. Numerical simulations of Kuo et al. for $\eta = 0.5$ [26] and Yang for $\eta = 0.8$ [27] have shown that the flow near the top end is different from that of the bottom. They have shown that at the top end, there exists a small corner vortex which may be the source of excitation of the traveling waves that amplify along the axial direction until they saturate near the bottom. In the experiment, it was difficult to visualize this corner vortex because of its weakness for the range of values of working parameters.

We may mention that this pattern is not induced by any inhomogeneities of the experimental setup: in fact, the radial heat flux across the gap is very weak ($Nu \sim 2$) compared to the vertical heat flux in the inner tube and between peripheral cylinders for which $Nu_1 = 82$ and $Nu_2 = 67$ respectively. So there is no vertical temperature gradient between the bottom and the top of the experimental setup.

5.2 Spiral vortices

The Couette-Taylor system with a radial temperature gradient has been subject of few experiments in systems with different geometrical parameters (η, Γ). We have gathered the characteristics of these experiments in Table 2 and we have plotted the critical values of these two experiments together with ours in the plane (Gr^*, Ta) where $Gr^* = \text{sgn } Gr \ \ln (Gr \ \text{sgn } Gr)$ in Figure 14. Snyder and Karlsson [8] found that for a small temperature gradient, the Couette flow was stabilized and the first instability gave rise to stationary Taylor vortices while a larger temperature gradient destabilizes the Couette flow leading to a spiral vortex pattern. Sorour and Coney [9] found that Couette flow was destabilized and a traveling vortex flow was observed. None of these authors had mentioned the occurrence of vortices near the bottom of the flow system although all the experiments have been performed in large aspect ratio systems. It is possible that the threshold was chosen to correspond to the state when the pattern filled the whole system. The Grashof values in Snyder and Karlsson's experiment are smaller than ours for the same temperature difference intervals because of smaller value of their gap. Sorour and Coney used oils with high viscosity (high Prandtl number) so giving small Grashof numbers. The difference in the critical values of Ta may also be due to the different values of the radius ratio, such a difference exists also in the isothermal case. While our results showed that the pattern wavenumber varied with the temperature gradient, Snyder and Karlsson reported that the wavenumber was almost independent of the latter. The inclination of vortices in closed flows implies both propagation in axial and azimuthal directions: $c_z = c_\theta \ \tan\theta$, where θ is the inclination angle. We have found that the axial phase velocity of spiral vortices was given by $c_z = 2.9 \times 10^{-3} W_a \approx W_{max}/3$, this value is almost independent of Ta. Snyder and Karlsson found that the axial phase velocity was comparable with the maximum of the axial velocity $c_z \sim W_{max}$. The spiral pattern rotates in the azimuthal direction with an angular velocity (ω/m) which is determined by the inner cylinder rotation. In fact, it has been shown theoretically that the spiral frequency is scaled by the mean rotation rate of the circular Couette flow as follows [28,29]:

$$\frac{\omega}{m} = \Omega \quad , \quad \Omega = \alpha(\eta)\Omega_i \ \tau_\nu \tag{4}$$

where the function α is given by [28,29]:

$$\alpha(\eta) = -\frac{2\eta^2}{1-\eta^2}\left(\frac{1}{2} + \frac{\ln \eta^2}{1-\eta^2}\right). \tag{5}$$

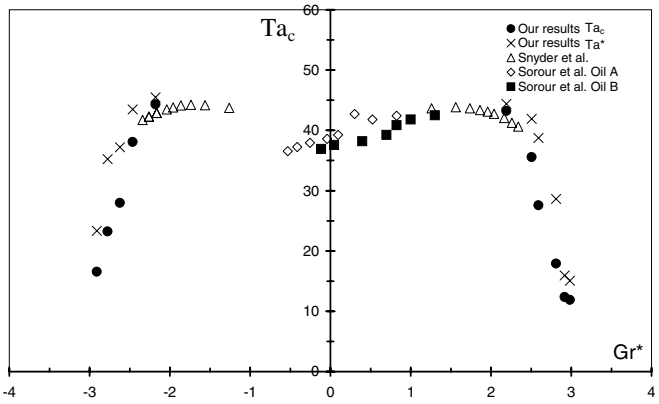

Fig. 14. Comparison of experimental studies: Snyder and Karlsson ($\eta = 0.958$), Sorour and Coney ($\eta = 0.948$) with two oils and our results ($\eta = 0.8$).

For our experiment, we have $\alpha(\eta = 0.8) = 0.426$ and the straight line fit of the experimental data in Figure 10 gives $\alpha(\eta = 0.8) = 0.428$. For Snyder and Karlsson system $\eta = 0.958$ and $\alpha(\eta) = 0.486$, this value is very close to values $\alpha \simeq 0.5$ reported in their article (see their Tab. 4). The pattern time-averaged frequency does not depend on the axial position. The time-averaged wavenumber is sensitive to the position because the amplitude is modulated in space which can be considered as a consequence of the control parameter ramp [30].

The stability of the Couette flow with a radial temperature gradient has been subject of few theoretical studies for different values of the radius ratio [10,31] and infinite system and of numerical studies for $\eta = 0.5$ and aspect ratio $\Gamma = 10$ [26]. Since the theoretical studies used infinite aspect ratio system and the numerical studies used the periodic boundary conditions, they could not recover any specific behavior of the pattern near $z = 0$ or $z = L$. This behavior should be recovered by numerical simulations with real physical boundary conditions.

5.3 Wall mode

The pattern observed in our experiment is composed of spirals drifting along the axial direction. Most of its properties can be described by the 1-d complex Ginzburg-Landau equation for the envelope amplitude $A(t, z)$ with homogenous boundary conditions:

$$\tau_0\left(\frac{\partial A}{\partial t} + v_g \frac{\partial A}{\partial z}\right) = \mu A + \xi_0^2(1 + ic_1)\frac{\partial^2 A}{\partial z^2} - g(1 + ic_2)|A|^2 A$$
$$A(z = 0) = A(z = L) = 0$$

where τ_0 is the characteristic time of the amplitude, v_g is the group velocity, ξ_0 is the coherence length, g is the Landau saturation constant, c_1 is the linear dispersion coefficient, and c_2 represents the nonlinear frequency detuning. For some systems e.g. Rayleigh-Bénard, Couette-Taylor, these coefficients can be computed in numerical simulations [32,33,36] or estimated in experiments [37,38], but

Table 2. Comparison of characteristics of some experiments.

Authors	η	Γ	Fluid	Pr	Gr
Snyder et al. [8]	0.958	337	water	4.35	$[-360; 360]$
	0.958	337	water	5.79	$[-360; 360]$
	0.958	337	1/3 glycerine-2/3 water	18.81	$[-360; 360]$
Sorour et al. [9]	0.911	60	oil A	[300;500]	
	0.911	60	oil B	[500;860]	
	0.948	102	oil A	[300;500]	[−3.5;0]
	0.948	102	oil B	[500;860]	[−3.5;0]
Ball et al. [7]	0.437	31.4	air	0.7	
	0.565	52.53	air	0.7	
	0.656	77.20	air	0.7	
Our experiments	0.8	114	water	5.5	$[-810; 965]$

for the Couette-Taylor flow with a radial temperature gradient, no data are available to our best knowledge.

For small values of the control parameter, the amplitude profile can be represented by the function $A(z) = A_0 e^{-\alpha z} \sin(\pi z/L)$ where A_0 is the initial amplitude of the wave, the coefficient $\alpha = \tau_0 v_g/[2\xi_0^2(1 + c_1^2)]$ [11,39]. Tobias et al. have called this solution a *wall mode*. We have determined experimentally the coefficient α. Following the analysis of Tobias et al., we have assumed that the threshold μ corresponds to absolute instability and used the relation $\mu = \tau_0 v_g/[2\xi_0^2(1 + c_1^2)]$. From α and μ, we have deduced $\tau_0 v_g$. The maximal amplitude has been used as a measure of the coefficient g. The frequency variation with μ has allowed for determination of the ratio c_2/τ_0. Using the behavior of the amplitude near the wall $z = 0$, we have measured the pattern coherence length ξ_s and from the approximate relation $\xi_s = \xi_0^2/(\tau_0 v_g)$ given in [40] we deduced an estimate of ξ_0 and then c_1 from the value of α. The obtained data are presented in the Table 3.

The behavior of the wall mode can be analyzed following the analysis of Zielinska et al. [41] of the global mode. We plotted in Figure 15 the A/A_{max} vs. z/z_{max}. We have observed that the near-wall behavior is almost described by one curve while away from the wall, i.e. in the zone $z > z_{max}$, there are separate curves that deviate each from another as μ increases. This deviation is induced by the different behavior of z_{max} and $z_f = L_p$ as a function of μ: $z_{max} \sim \mu^{1/2}$ and $z_f \sim \mu$. This is a consequence of the ratio between the thermal gradient and the centrifugal force. In fact the front is due to the presence of the axial velocity induced by radial temperature gradient, while the inner cylinder rotation will reinforce the effect of the centrifugal force, so increasing the appearance of the vortices in the whole system.

This kind of spiral patterns drifting in 1-direction have been observed in other hydrodynamical systems such as the Couette-Taylor flow with counterrotating cylinders [2] or the Taylor-Dean [33–35].

We have shown that the convection cell induced by the radial temperature gradient was responsible of the existence of the wall mode. A similar situation was observed for the hydrothermal waves generated in bounded channel submitted to a horizontal temperature gradient [42] in which there is also a convection cell.

Table 3. Coefficients of Ginzburg-Landau for a pattern with $Gr = -420$.

g	$\tau_0 v_g$	ξ_0	c_2/τ_0	c_1
1.86 ± 0.24	-4.56	3.42	-2.8	0.98

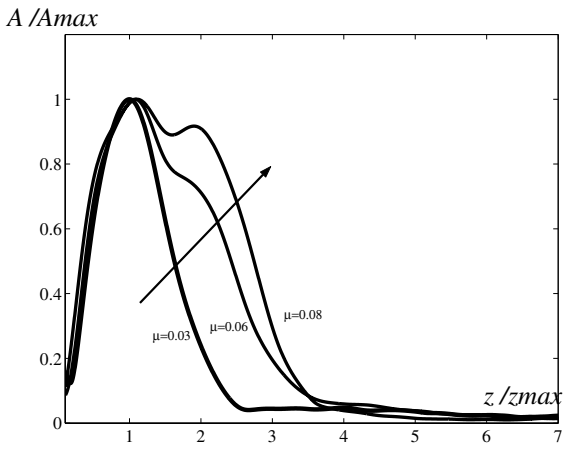

Fig. 15. Amplitude profiles A/A_{max} as a function of z/z_{max} of the traveling waves for $GR = -420$ and different values of μ.

5.4 Comparison with the Couette-Taylor system with a through flow

The investigated flow system has some analogy with the Couette-Taylor with an axial through flow [12–15,17,18]. In fact, the studied flow is composed of a circular Couette flow combined with a convection cell ascending near the hot wall and descending near the cold one. Far from the top and bottom boundaries, the base axial flow has a nodal surface separating the ascending from the descending flows, these two parts of the flow can be considered as axial flows in opposite directions. In order to compare with the Couette-Taylor system with a through flow whose one of the control parameter is the axial Reynolds number defined with the flow rate, we have used instead of the Grashof number (i.e. thermal Reynolds number) the axial Reynolds number expressed as follows:

$$Re = \frac{W_{max} d}{\nu} \tag{6}$$

where $W_{max} = F(\eta, r_{max}) W_a$ is the maximum velocity of the axial flow. The value of $F(\eta, r_{max})$ is given in Table 1 and for our experimental configuration, we have $Re = 8.4 \times 10^{-3}$ Gr. We have limited our analysis to small values of the axial Reynolds number $Re < 8$ (i.e. weak axial flow), so the buoyancy forces act as disturbances of the flow but are not sufficient enough to compete with the centrifugal force, responsible for the Taylor vortices. Figure 16 represents the averaged base flow position sometimes called *healing length* L_h as a function of the inverse of the reduced Taylor number. The laminar base flow disappears with the Taylor number in favor of the spiral vortex flow. The slope increases with the Grashof number (Fig. 16).

For Couette-Taylor with axial flow [13–15,17,18,43], the pattern occurred first at the outlet and was composed of propagating Taylor vortices (PTV) while the flow was still laminar at the inlet. So there is an interface separating the pattern state from the laminar state. This interface fluctuates in the convectively unstable region due to a spatial amplification of a permanent noise at the inlet [16]. The laminar zone was characterized by the healing length L_h which was found to diverge with the group velocity and so allowed for the determination of the onset of the regime of absolute instability. Increasing the rotation rate lead to the pattern filling the whole system.

In our system, the pattern is composed of spirals i.e. traveling non axisymmetric helicoidal vortices (Fig. 17) while the PTV were traveling but axisymmetric. The healing length of the pattern in both systems increases linearly with ϵ^{-1} (Fig. 16).

The interface between the PTV and the laminar state was described as fluctuating and therefore the pattern was referred to as "noise induced structures", we were not able to state this type of behavior for the interface in our case. We have found that the radial temperature gradient destabilizes the circular Couette flow while the axial flow stabilizes it. The analogy between these two systems needs for a further investigation, in particular, we need for a deep analysis of the convective and absolute instability regime in our case.

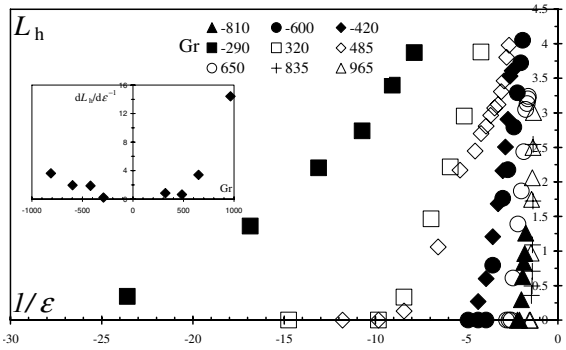

Fig. 16. Variation of the averaged base flow position L_h (part without rolls) vs. the inverse of the criticality parameter defined as $\epsilon = (Ta - Ta_c(Gr = 0))/Ta_c(Gr = 0)$ for different Grashof numbers. Variation of the slope $dL_h/d(1/\epsilon)$ vs. the Grashof number.

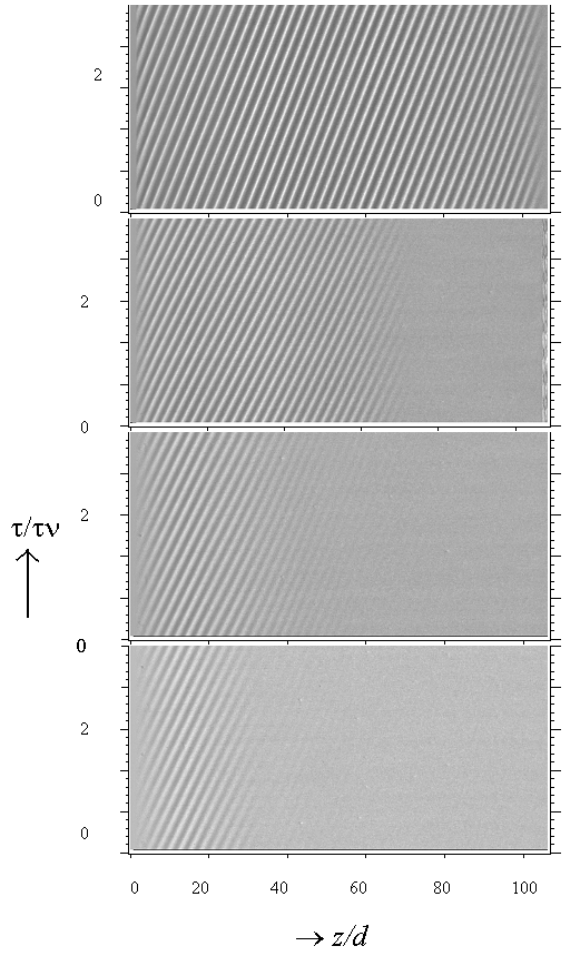

Fig. 17. Space-time diagrams obtained for $Re = -3.5$ and for different values of μ.

Table 4. Best fit coefficients of the critical parameters as functions of the axial Reynolds number. The starred quantities are the critical values for which the pattern fills the whole system.

X_c	a_1	a_2
Ta_c	$-3 \times 10^{-2} \pm 2 \times 10^{-3}$	$3.10^{-4} \pm 4 \times 10^{-5}$
Ta_c^*	$-0.013 \pm 6 \times 10^{-4}$	0
q_c	$-1.7 \times 10^{-2} \pm 2 \times 10^{-3}$	$1.2\ 10^{-4} \pm 5 \times 10^{-5}$
q_c^*	$-1.3 \times 10^{-2} \pm 2 \times 10^{-3}$	$8.10^{-5} \pm 4 \times 10^{-5}$
Y_c	b_1	b_2
f_c	0.91 ± 0.05	$8.4 \times 10^{-3} \pm 1 \times 10^{-3}$
f_c^*	0.69 ± 0.05	$-4.2 \times 10^{-3} \pm 1 \times 1\ 10^{-3}$

5.5 Variation of critical parameters with Re

We have observed that the spiral helicity depends on the sign of $GrTa \sim ReTa$, a similar conclusion was obtained by Ali and Weidman [10].

Analysis of a dependence of critical parameters with Gr (Figs. 6, 7–8) suggests the existence of a symmetry with respect to the sign of the temperature gradient. We have investigated the behavior of the critical parameters as function of the axial Reynolds number Re defined by (7) and we have found that Ta_c, Ta_c^*, q_c, q_c^* are even functions of Re

$$X_c(Re) = X_c(0)(1 + a_1 Re^2 + a_2 Re^4) \tag{7}$$

while f_c, f_c^* are odd function

$$Y_c(Re) = b_1 Re + b_2 Re^3 \tag{8}$$

The best fit coefficients are presented in the Table 4.

Similar results were obtained for the Couette-Taylor system with axial flow in experiments and in numerical simulations [13,17,36].

6 Conclusion

We have investigated the effects of a weak radial temperature gradient on the stability of the Couette flow. We have found that the radial temperature gradient amplifies the destabilization of the base flow. A pattern of traveling inclined vortices (spirals) occurred near the bottom of the annular cavity for the rotation frequency below the threshold of the Taylor vortices. The pattern increases in size with the increase of the control parameter before invading the whole cavity. For a range of values of the control parameter Ta, the spiral pattern coexists with the laminar flow. The size of the laminar flow, i.e. the healing length decreases with Ta, the slope of this variation depends on Gr. A similar behavior has been observed in the Couette-Taylor system with an axial flow. We have also noticed that the radial heating increases the axial size, the inclination and the drift velocity of vortices.

The spiral pattern observed in this system is a good candidate for a description by the 1D complex Ginzburg-Landau equation for which we have determined the coefficients. The results have been performed for a temperature difference below $|2|^\circ$ C corresponding to an axial Reynolds number $|Re| \in [0, 8.5[$ in order to consider the radial heating as a small perturbation. A comparison with noise induced pattern in the Couette flow with axial through flow has been performed. For larger temperature differences, there is a strong coupling between the buoyancy and centrifugal effects that leads to new instability modes. Corresponding results will be presented elsewhere.

We thank Olivier Crumeyrolle for fruitful discussions. This work is supported partially by the CPER 2000-2006 under the program CNRT-Maîtrise de la Combustion dans les Moteurs. V.L. and A.G. had benefited from financial support of the French Ministry of Research.

References

1. R.C. DiPrima, H.L. Swinney, *Hydrodynamic Instabilities and the Transition to Turbulence*, edited by H.L. Swinney, J.P. Gollub (Springer New York, 1985), p. 139
2. C.D. Andereck, S.S. Liu, H.L. Swinney, J. Fluid Mech. **164**, 155 (1986)
3. R. Tagg, Nonlinear Sci. Today **4**, (1994)
4. F. Kreith, *Convection heat transfer in rotating systems*, in Advances in Heat Transfer, edited by T.F. Irvine, J.P. Hartnett (Academic Press, New York, 1968), Vol. 5, p. 129
5. Y.N. Lee, W.J. Minkowycz, Int. J. Heat Mass Transfer **32**, 711 (1989)
6. P.H. Singer, Semiconductor International **72** (1984)
7. K.S. Ball, B. Farouk, V.C. Dixit, Int. J. Heat Mass Transfer **32**, 1517 (1989)
8. H.A. Snyder, S.K.F. Karlsson, Phys. Fluids **7**, 1696 (1964)
9. M.M. Sorour, J.E.R. Coney, J. Mech. Eng. Sci. **21**, 403 (1979)
10. M. Ali, P.D. Weidman, J. Fluid Mech. **220**, 53 (1990)
11. S.M. Tobias, M.R.E. Proctor, E. Knobloch, Physica D **113**, 43 (1998)
12. H.A. Snyder, Proc. R. Soc. London, Ser. A **265**, 198 (1962)
13. A. Tsameret, V. Steinberg, Phys. Rev. Lett. **67**, 3392 (1991)
14. A. Tsameret, V. Steinberg, Europhys. Lett. **14**, 331 (1991)
15. A. Tsameret, G. Goldner, V. Steinberg, Phys. Rev. E **49**, 1309 (1994)
16. A. Tsameret, V. Steinberg, Phys. Rev. E **49** 2, 1291 (1994)
17. K.L. Babcock, G. Ahlers, D.S. Cannell, Phys. Rev. Lett. **67**, 3388 (1991)
18. J.B. Swift, K.L. Babcock, P.C. Hohenberg, Physica A **304**, 625 (1994)
19. P.G. Drazin, W.H. Reid, *Hydrodynamic Stability* (Cambridge University Press, 1991)
20. V. Lepiller, A. Prigent, F. Dumouchel, I. Mutabazi, Phys. Fluids **19**, 054101 (2007)
21. P. Matisse, M. Gorman, Phys. Fluids **27**, 759 (1984)
22. H. Litschke, K.G. Roesner, Exp. Fluids **24**, 201 (1998)

23. A. Prigent, O. Dauchot, Phys. Fluids **12**, 2688 (2000)
24. V. Croquette, H. Williams, Physica D **37**, 300 (1989)
25. J. Walowit, S. Tsao, R.C. DiPrima, J. Appl. Mech., Trans. ASME **31** Series E, 585 (1964)
26. D-C. Kuo, K.S. Ball, Phys. Fluids **9**, 2872 (1997)
27. K.-S. Yang, Private Communication
28. F. Caton, B. Janiaud, E.J. Hopfinger, J. Fluid Mech. **419**, 93 (2000)
29. Ch. Hoffman, M. Lücke, A. Pinter, Phys. Rev. E **69**, 056309 (2004)
30. M.A. Dominguez-Lerma, D.S. Cannell, G. Ahlers, Phys. Rev. A **34**, 4956 (1986)
31. M. Ali, G.B. McFadden, Phys. Fluids **17**, 054112.1 (2005)
32. Y. Demay, G. Iooss, J. Mec. Theor. Appl. (Special Issue), 193-216 (1984)
33. P. Laure, I. Mutabazi, Phys. Fluids **6**, 3630 (1994)
34. P. Bot, O. Cadot, I. Mutabazi, Phys. Rev. E **58**, 3089 (1998)
35. P. Bot, I. Mutabazi, Eur. Phys. J. B **13**, 141 (2000)
36. A. Recktenwald, M. Lücke, H.W. Müller, Phys. Rev. E **48**, 4444 (1993)
37. J. Burguete, H. Chaté, F. Daviaud, N. Mukolobwiez, Phys. Rev. Lett. **82**, 3252 (1999)
38. A. Goharzadeh, Ph.D. thesis, University of Le Havre, 2001
39. R.J. Deissler, Phys. Fluids **30**, 2303 (1987)
40. M.C. Cross, Phys. Rev. A **38**, 3593 (1988)
41. B.J.A. Zielinska, D. Mukamel, V. Steinberg, Phys. Rev. A **33**, 1454 (1986)
42. N. Garnier, A. Chiffaudel, F. Daviaud, Phys. Rev. Lett. **88**, 134501 (2002)
43. R.M. Lueptow, A. Docter, K. Min, Phys. Fluids A **4**, 2446 (1992)